Reconstruction of three-dimensional biventricular activation based on the 12-lead ECG via patient-specific modeling

Authors: Simone Pezzuto, PhD[1]; Frits W Prinzen, PhD[2]; Mark Potse, PhD[3,4,5]; Francesco Maffessanti, PhD[1]; François Regoli, MD[1,6]; Maria Luce Caputo, MD[1,6]; Giulio Conte, MD, PhD[1,6], Rolf Krause, PhD[1]; Angelo Auricchio, MD, PhD[1,6].

[1]Center for Computational Medicine in Cardiology, Institute of Computational Science, Università della Svizzera italiana, Lugano, Switzerland

[2]Dept. of Physiology, CARIM, Maastricht University, Maastricht, The Netherlands

[3]Univ. Bordeaux, IMB, UMR 5251, Talence, France

[4]CARMEN Research Team, Inria Bordeaux - Sud-Ouest, Talence, France

[5]IHU Liryc, fondation Bordeaux Université, Pessac, France

[6]Division of Cardiology, Fondazione Cardiocentro Ticino, Lugano, Switzerland

Word count (excluding tables and references): 3491 (max. 3500)

References: 19 (max. 20)

Short title: Activation reconstruction from 12-lead ECG

Address of correspondence:

Simone Pezzuto, PhD

Center for Computational Modeling in Cardiology,

Institute of Computational Science, Università della Svizzera italiana,

Via Giuseppe Buffi 13, CH-6904 Lugano, Switzerland

E-mail: simone.pezzuto@usi.ch

Phone (office): +41 58 666 4976

Structured Abstract

Aims. Non-invasive imaging of electrical activation requires high-density body surface potential mapping. The 9 electrodes of the 12-lead ECG are insufficient for a reliable reconstruction with standard inverse methods. Patient-specific modeling may offer an alternative route to physiologically constraint the reconstruction. The aim of the study was to assess the feasibility of reconstructing the fully 3D electrical activation map of the ventricles from the 12-lead ECG and magnetic resonance (CMR).

Methods. Ventricular activation was estimated by iteratively optimizing the parameters (conduction velocity and sites of earliest activation) of a patient-specific model to fit the simulated to the recorded ECG. Chest and cardiac anatomy of 11 patients (QRS duration 126-180 ms, documented scar in two) were segmented from CMR images. Scar presence was assessed by MR contrast enhancement. Activation sequences were modelled with an eikonal equation and ECGs with lead field theory. Validation was performed by comparing reconstructed activation maps with invasive electroanatomical mapping of the coronary sinus/veins (CS) and the right (RV) and left ventricular (LV) endocardium.

Results. The QRS complex was correctly reproduced by the model (Pearson's correlation r=0.923). Reconstructions accurately located the earliest and latest activated LV regions (median barycenter distance 8.2 mm, IQR 8.8 mm). Correlation of simulated to recorded activation was very good at LV endocardium (r=0.83), and good at CS (r=0.68) and RV endocardium (r=0.58).

Conclusion. Non-invasive assessment of biventricular 3D activation using the 12-lead ECG and MR imaging is feasible. Potential applications include patient-specific modeling and pre-/per-procedural evaluation of ventricular activation.

Keywords. 12-lead ECG; 3D activation; eikonal model; patient-specific modelling

Condensed abstract

A model-based reconstruction of the three-dimensional activation map relying only on the 12-lead ECG and patient-specific anatomy was investigated. The reconstruction was achieved by fitting the parameters of a patient-specific model (conduction velocity, sites of earliest activation) to the recorded ECG. In 11 patients, the method correctly reproduced the surface QRS complex. The reconstructed activation map correlated strongly with the invasive electroanatomical mapping.

What's new?

- Reconstruction of 3D activation map with only 12-lead ECG, patient-specific anatomy and CMR-derived scar using an eikonal model for the electric activation
- Validation of reconstruction against RV and LV endocardial, and LV epicardial invasive, high-density electroanatomic maps in 11 patients
- Physiologically accurate conduction with heterogeneities (scar, fast endocardial layer) and anisotropy (fibers)
- Enabling technology for non-invasive individualization of patient-specific models

Introduction

The standard 12-lead electrocardiogram (ECG) is the most routinely used, inexpensive and non-invasive modality to record the electrical activity of the heart, but its diagnostic capability has acknowledged limits. In particular, the surface ECG does not provide quantitative information about the activation sequence in the heart.

Non-invasive electrocardiographic imaging, also called ECG mapping, overcomes at least some of the limitations of the standard ECG. ECG mapping combines information from many (usually 150-250) electrodes with knowledge of the geometry of the heart and torso of the patient to depict the electric activity of the heart.[1] It is a general-purpose tool that can reconstruct potentials, electrograms, and activation and repolarization patterns on either the epicardium or, less commonly, the endocardium. Some technologies based on ECG mapping have been extensively validated in experimental, animal and clinical studies, with convincing results.[2–5] However, ECG mapping relies on a large number of electrodes, placed on the patient's torso at the time of geometry acquisition using cardiac imaging as well as during the clinical intervention, thus requiring dedicated technical support and additional costs. Therefore, despite the advantages, its adoption in the clinical workflow is still limited.

In the present study we assess the possibility to reconstruct the activation map relying only on the 12-lead ECG for the electric data, by taking advantage of physiological and anatomical knowledge implemented in a patient-specific model. The parameters of the model, regional conduction velocities and sites of earliest activation, are automatically optimized to fit the simulated to the recorded ECG. The fitted patient-specific model can calculate almost real-time the activation sequence and may therefore enable model-assisted therapeutic intervention. Proof-of-principle validation was performed on a small, yet heterogeneous cohort of patients possibly with a scar by an extensive comparison of the calculated activation map against the invasively acquired high-density electro-anatomic endocardial map.

Methods

Study population

Eleven heart failure patients were retrospectively included in the study. A 12-lead ECG, a clinically indicated magnetic resonance (MR) scan with late gadolinium-enhancement (LGE), and an electrophysiological study including an electroanatomic mapping (EAM) procedure were performed in all the patients before device implantation (see supplemental material). The institutional review board approved the study protocol, and all patients gave written and oral informed consent for the investigation. The study was performed in compliance with the Declaration of Helsinki.

Construction of the patient-specific model

Figure 1 shows the overall workflow from data acquisition to model construction and validation. The eikonal model for simulating myocardial activation and body surface ECG has been previously described.[6] In summary, the electrical activation originated from a limited number (1 to 10) of early activation sites (EASs) and spread across the active myocardium with given spatially varying, direction-dependent conduction velocity. The propagation was faster in the fiber direction than in the cross-fiber direction. Scar was modeled as non-conductive tissue. The QRS complex of the 12-lead ECG was simulated by using the formula:

$$V_k(t) = \int_\Omega \boldsymbol{G}_{in}(x) \nabla U(t - \tau(x)) \cdot \nabla Z_k(x) \, dx,$$

which combines the lead fields in the torso $Z_k(x)$, one per lead $k = 1, \dots, 12$, and a template action potential $U(t)$ shifted in time according to activation onset $\tau(x)$. The integration domain Ω was the 3D active myocardial tissue, with intracellular conductivity tensor $\boldsymbol{G}_{in}(x)$. For the computation of the lead fields, the torso included lungs, blood masses, active and non-conductive myocardium (with anisotropy), skeletal muscles, and skin. Further details on the construction of the anatomical model and the computation of the lead fields are available in the supplemental material.

In order to reproduce the recorded QRS complex, the number of EASs, along with their locations and onsets, and the conduction velocity in 4 distinct regions (LV, RV and LV, RV fast endocardial layer) were automatically adapted to minimize the least-squares error between the simulated and recorded QRS complexes. Several other parameters (electric

6

conductivities, membrane model) were left unchanged from those reported in previous

studies. The initial guess for the optimized parameters was the same in all the patients.

The minimization procedure consisted of 2 phases. The first phase optimized the global CV

and number of EASs, along with an initial estimate of their location and activation onset.

Simulations started with at least 100 tentative EASs uniformly distributed across the LV and

RV endocardium (excluding scar), all simultaneously activating with zero onset and with

fixed location along the whole procedure. The optimization of the parameters proceeded

iteratively as follows: firstly, onsets of all EASs were optimized to locate the region of

earliest activation; secondly, a shift-and-scale transformation of the activation map, obtained

by adjusting CV and onset, aimed for an optimal alignment of simulated and recorded ECG;

thirdly, EASs with negligible impact on the activation map (in terms of region of influence)

were progressively removed. The three steps were iterated until no further reduction in the

error was possible. In the second optimization phase the number of EASs was fixed whereas

their location and onset were optimized in combination with the local CV, until convergence.

Validation

EAMs and patient-specific anatomy were aligned by means of a translation and the acquired

points were projected onto the corresponding anatomical region (LV or RV endocardium, LV

epicardium). Validation was performed by comparing the recorded and reconstructed

activation time both pointwise and regionally. The LV earliest and latest activated regions

(EAR and LAR) were presented using a bull's-eye plot. The EAR and LAR were respectively

defined as the earliest 10% and the latest 10% of activated endocardium. The endocardial

breakthrough point (BP) and latest activated point (LAP) were defined as the projected

barycenter of the EAR and LAR, respectively. A trans-septal time (TST) was defined as the

earliest LV breakthrough time, whereas the total activation time (TAT) was the latest

activation time within the LV endocardium. The overlap (OVL) between recorded and

reconstructed activation was evaluated as area of the overlap when 20% of the total

endocardium was activated, divided by 0.2.

Statistical analysis

Recorded and simulated ECG were compared in terms of Pearson's correlation, relative root-

mean-square error (RMSE) and QRS duration. A similar analysis was applied to the

pointwise comparison to EAMs. All distances were computed using the Euclidean distance.

153   All quantities are reported in mean ± SD, or median and 1st and 3rd quartile, if not indicated

154   differently.

155

Results

A summary of the demographic characteristics of the included patients is shown in Table 1. On average 265±109 endocardial activation points per patient were acquired. In 11 patients, 186±59 LV endocardial points were collected, in 6 patients an additional 71±22 points in the RV, and in 7 patients 63±19 points were recorded on the LV epicardium by introducing the mapping catheter into the coronary sinus and whenever possible in the coronary veins.

Detection of EASs

An illustrative example of the fitted patient-specific models is reproduced in Figure 2 for an IVCD patient with coronary artery disease (patient #4). The patient has a non-LBBB QRS morphology and an extensive sub-endocardial scar located in the LV antero-lateral wall. The algorithm identified 14 EASs, 7 RV and 7 LV. No RV-LV delay was observed. In the LV, BPs were in the septal area both inferiorly and anteriorly, with a slightly higher occurrence in the inferior sectors. The simulated and recorded QRS complexes correlated excellently (r= 0.978). The BP and LAP localization errors were 11.1 mm and resp. 8.9 mmm respectively. Notably, 4 EARs were correctly identified, with 2 EARs in the antero-septal area and 2 EARs in the inferior-septal area, very close to the recorded EAR in the same area. Pointwise correlation between calculated and measured points was 0.78 and OVL 0.4.

Overall accuracy of reconstructed activation

A pointwise comparison of reconstructed activation at points from EAM (Table 2) showed very high Pearson's correlation (r=0.815), particularly at LV endocardium (r=0.833). In the RV endocardium and coronary sinus/veins the correlation was lower (r=0.576 and r=0.677). The Bland-Altman analysis showed no bias (0.45 ms) and limits of agreement (LoA) of −42.7 ms and +43.6 ms (2856 points). On the LV epicardium and endocardium, the reconstruction was good (r>0.7) in 10 patients (91%) and modest only in patient #3 (r=0.33). On the RV endocardium Pearson correlation per patient was generally modest (r>0.5 in 4 patients out of 6) and poor in patient #6 (r=0.18). A relatively large bias of 27 ms was observed on the RV endocardium with LoA −18 ms and 72 ms.

The estimated TST obtained from the fitted model closely matched the measured TST (difference between reconstructed and recorded was −15.5±16.5 ms) in all but one. The reconstructed TAT slightly overestimated the recorded one, with a difference of 25.7±22 ms.

9

186   The BP and LAP in the LV were accurately identified in the correct AHA sector on

187   the bull's-eye plot in the majority of the patients (72%). In the remaining cases, BP was

188   placed in the neighbor segments (Figure 3). The distance between the calculated and the

189   recorded BP was 13.5 [6.9,16.1] mm, and the OVL was 0.75 [0.56,0.79]. The LAP was also

190   accurately captured by the reconstructed activation map, 8.1 [6.1,14.5] mm off the recorded

191   position.

192   **Accuracy of fitting the ECG**

193   Overall, the fitted QRS complex was highly correlated to the recorded QRS complex (r=0.92)

194   and correlation was >0.9 in 9 out of 11 patients (82%). Per-patient correlation (Table 3)

195   ranged from 0.84 (patient #7) to 0.98 (patient #6). The QRS duration was well captured,

196   reporting an error (reconstructed minus recorded) of −3.0 [−17.37,5.28] ms. Overall, V1-V4

197   showed very high correlation while lead V6 and aVR showed modest correlation.

198

Discussion

This study shows that a mathematical model can accurately reconstruct the volumetric propagation sequence of the ventricles in heart-failure patients. In contrast to commercially available ECG mapping technologies, it does not require hundreds of electrodes; we obtained our results with only the 12-lead ECG and standard imaging data. The method can be easily integrated in existing EAM systems, possibly reducing mapping time, and increasing localization accuracy.

Our method is neither the first to require only a 12-lead ECG,[7,8] nor the first to predict the activation sequence in the entire ventricular volume,[9] but it is the first to achieve both of these feats without compromising the physiological accuracy or strongly limiting the applicability of the approach. Our method combines the best of two worlds: ECG mapping[1,2,7,9] and patient-specific modeling.[10–12] Due to a highly optimized implementation the reconstruction is competitive in terms of time to solution to other ECG mapping approaches. At the same time, the accuracy of its ECG prediction is comparable to the gold standard, the bidomain model.[6] We achieve this accuracy by using a volumetric conduction model, necessary to incorporate the effect of tissue anisotropy on the potential field generated by the activation wavefront. This automatically results in a fully 3D prediction of the activation sequence. The activation sequence itself was simulated realistically with an anisotropic eikonal equation. Importantly, we did not observe potentially unphysiological lines of block and U-shaped activation, often present in ECG mapping, because conduction velocity cannot change abruptly unless directly specified in the model. Particularly relevant is the presence in our model of a thin, fast endocardial layer in the LV and RV, which better captures the physiological behavior in this region.[13]

Accuracy

We quantified the accuracy of the reconstruction as the correlation of invasively measured and calculated activation times, their timing difference and the precision of locating the early and late activated regions. Commercially-available ECG mapping systems, while extensively tested in experimental and animal studies, have been validated in a clinical setting with these metrics only very recently and still with a limited coverage of RV and LV endocardium.[3,5,15,16] The patient population in the present study included patients with

11

coronary artery disease and a wide range of QRS duration and morphology, which in the vast majority of studies of standard ECG mapping systems was missing.

The overall correlation of the activation map in the present study (r=0.82) is comparable to those reported for ECG mapping in controlled isolated hearts (r=0.68±0.265), in-vivo animal experiments (r=0.82), and in clinical studies during pacing (r=0.66).[3,4,15] Studies performed during sinus rhythm, better reflecting our cohort, showed significantly lower correlation (r close to zero).[15] Similarly, our localization error of BP and LAP in the LV (12.2±8.8 mm) compared well with those of the animal studies (9.1±0.6 and 10 mm, respectively) and is much better than those reported in the clinical study in sinus rhythm.[15] In the analysis we also considered the similarity (in terms of overlap) between recorded and reconstructed earliest activation (0.69±0.17) as a metric for accuracy in the reconstruction. While a small localization error suggests an accurate reconstruction of BP and LAP location, a large overlap indicates that conduction properties are also correct.

The reconstruction of the CS/veins map adequately reproduced the invasive recordings. In contrast, the RV activation reconstruction was modest in terms of correlation (r=0.58) and showed on average a deviation from the EAM of 27 ms. A closer inspection of the Bland-Altman plot suggests that points in the earliest activated region were well reproduced while late-activated points were considerably delayed in the reconstructed map. The RV contributes less than the LV to the ECG, and the least-squares minimization used here tends to ignore small deviations in amplitude, hence limiting the accuracy. Additionally, the alignment of the recorded RV points to the anatomy is problematic and may be affected by large uncertainty, because of the concave shape of the chamber.

Patient-specific modelling

By virtue of its model-based nature, our approach has the potential to further improve the individualization in patient-specific modelling, an emerging paradigm aiming at supporting personalized therapeutic interventions.[17] Non-invasive mapping of ectopic foci and personalization of cardiac models from 12-lead ECG has already been investigated by others.[7,8,10–13] These methods are accurate but often rely on the somewhat restrictive assumption that only a single EAS is to be identified. We overcome this assumption with a novel strategy to identify an optimal number and location of sites of earliest activation.

Robustness of validation

The activation map extrapolated from the invasive mapping system may be affected by several uncertainties. The detection of the activation time from EGM could be difficult because of fractionation and far field signal in the unipolar readings, and direction-dependency in bipolar signals.[18] In addition, the spatial location of imaged points needs to be registered to the electrode positions. The combination of both these uncertainties (in space and in time) may affect the comparison, especially for BP and LAP localization. In this work we opted for the more robust definition of BP (resp. LAP) as the barycenter of the EAR (resp. LAR). In a Monte Carlo study, we found that the localization error of BP has significantly lower variance if defined as above instead as the earliest activated point. (See supplemental material.)

Perspectives on clinical application

Our method could be included in the screening workflow of patients who are candidate to CRT as well as in selecting pacing targets. The measurement of the time interval between RV and LV, or the time between Q wave on surface ECG and LV at the time of CRT implantation has been predictive of both acute and chronic response to CRT.[19] The method could easily estimate both RV-LV timing and Q-LV time and thus provide a novel way for patient selection and pre-procedural planning of RV and LV lead placement. Patient-specific activation patterns can be calculated right at the time of pacing lead placement.

Study limitations

The patient-specific model has several parameters with considerable uncertainty. This is an undeniable problem of current cardiac models and, more generally, biological systems. The objective function is highly non-linear and non-convex with respect to the parameters of the model, hence given the limited amount of data we use for the fitting, it is plausible that multiple combinations of parameters yield similar activation maps and surface ECG. The solution may therefore depend on the initial guess for the parameters and the optimization algorithm. In order to alleviate this problem, we designed the first phase of the algorithm to provide a possible initial guess. More advanced global optimization techniques may offer a more robust approach, albeit with a higher computational footprint.

The eikonal model does not cover the full spectrum of activation patterns. This may limit its applicability. Most notably, reentrant activation is not admissible in our current formulation.

The study was admittedly based on a small patient cohort. However, this cohort was heterogeneous, with QRS duration ranging from 126 to 180 ms, different ventricular conduction abnormalities and variable underlying disease (e.g. scar). Importantly, the validation measurements consisted of high-resolution endocardial mapping in both ventricles and epicardial LV measurements in heart failure patients. In contrast, the majority of the previous ECG imaging studies have only considered epicardial data during SR, endocardial data with pacing from a single site, or data derived from in silico models.

The validation analysis in this study was not performed blindly to the intracardiac mapping. To avoid a possible bias, we employed the same initial guess in the algorithm for all the patients, despite the heterogeneity of the cohort.

Currently, the model requires an accurate segmentation and mesh-construction from imaging data, which may require several hours per patient. For the majority of applications, a preparatory phase of several hours is reasonable and it does not disrupt the clinical workflow. Nonetheless, time to segmentation can nowadays be improved significantly by a combination of statistical atlases and machine learning.

Finally, scar was assessed by LGE-MRI acquisitions, which might not be routinely available. We also did not consider the border zone of the scar in the model, although the model can easily allow for it.

Conclusions

A 12-lead ECG-based technique for reconstructing cardiac activation was developed and validated. The methodology achieved very good endocardial accuracy, opening the possibility for a non-invasive pre- and peri-procedural evaluation of activation map during intrinsic sinus rhythm and, potentially, for guiding optimal lead placement.

Disclosures: AA is consultant with Boston Scientific, Backbeat, Biosense Webster, Cairdac, Corvia, Daiichi-Sankyo, Medtronic, Merit, Microport CRM, Philips, and V-Wave; received speakers' fee from Daiichi-Sankyo, Boston Scientific, Biosense Webster, Medtronic, Microport CRM, and Philips; participates in clinical trials sponsored by Boston Scientific, Medtronic, Microport CRM, and Zoll Medical; and has intellectual properties assigned to Boston Scientific, Biosense Webster, and Microport CRM. FP has received research grants from Medtronic, Abbott, Microport CRM, Biotronik and Biosense Webster and speakers fee from Medtronic, Abbott and Microport CRM; and he reports intellectual property with Boston Scientific, Medtronic and Biosense Webster. FM reports intellectual property with Biosense Webster. FR is consultant for Daiichi-Sankyo, Medtronic, and Bayer. All the other authors have nothing to disclose.

Data availability: The data underlying this article cannot be shared publicly for the privacy of individuals that participated in the study. The data will be shared on reasonable request to the corresponding author.

References

1. Ramanathan C, Ghanem RN, Jia P, Ryu K, Rudy Y. Noninvasive electrocardiographic imaging for cardiac electrophysiology and arrhythmia. *Nat Med* 2004;**10**:422–8.

2. Berger T, Fischer G, Pfeifer B, Modre R, Hanser F, Trieb T, *et al.* Single-Beat Noninvasive Imaging of Cardiac Electrophysiology of Ventricular Pre-Excitation. *J Am Coll Cardiol* 2006;**48**:2045–52.

3. Cluitmans MJM, Bonizzi P, Karel JMH, Das M, Kietselaer BLJH, Jong MMJ de, *et al.* In Vivo Validation of Electrocardiographic Imaging. *JACC Clin Electrophysiol* 2017;**3**:232–42.

4. Bear LR, LeGrice IJ, Sands GB, Lever NA, Loiselle DS, Paterson DJ, *et al.* How Accurate Is Inverse Electrocardiographic Mapping? *Circ Arrhythmia Electrophysiol* 2018;**11**:1–12.

5. Graham AJ, Orini M, Zacur E, Dhillon G, Daw H, Srinivasan NT, *et al.* Simultaneous Comparison of Electrocardiographic Imaging and Epicardial Contact Mapping in Structural Heart Disease. *Circ Arrhythmia Electrophysiol* 2019;**12**:e007120.

6. Pezzuto S, Kal'avský P, Potse M, Prinzen FW, Auricchio A, Krause R. Evaluation of a Rapid Anisotropic Model for ECG Simulation. *Front Physiol* 2017;**8**:265.

7. Misra S, Van Dam P, Chrispin J, Assis F, Keramati A, Kolandaivelu A, *et al.* Initial validation of a novel ECGI system for localization of premature ventricular contractions and ventricular tachycardia in structurally normal and abnormal hearts. *J Electrocardiol* Elsevier Inc; 2018;**51**:801–8.

8. Alawad M, Wang L. Learning domain shift in simulated and clinical data: Localizing the origin of ventricular activation from 12-lead electrocardiograms. *IEEE Trans Med Imaging* IEEE; 2019;**38**:1172–84.

9. Han C, Pogwizd SM, Killingsworth CR, He B. Noninvasive imaging of three-dimensional cardiac activation sequence during pacing and ventricular tachycardia. *Heart Rhythm* 2011;**8**:1266–72.

10. Villongco CT, Krummen DE, Stark P, Omens JH, McCulloch AD. Patient-specific modeling of ventricular activation pattern using surface ECG-derived vectorcardiogram

in bundle branch block. *Prog Biophys Mol Biol* Elsevier Ltd; 2014;**115**:305–13.

11. Zettinig O, Mansi T, Neumann D, Georgescu B, Rapaka S, Seegerer P, *et al.* Data-driven estimation of cardiac electrical diffusivity from 12-lead ECG signals. *Med Image Anal* Elsevier B.V.; 2014;**18**:1361–76.

12. Giffard-Roisin S, Delingette H, Jackson T, Webb J, Fovargue L, Lee J, *et al.* Transfer learning from simulations on a reference anatomy for ECGI in personalized cardiac resynchronization therapy. *IEEE Trans Biomed Eng* 2019;**66**:343–53.

13. Lee AWC, Nguyen UC, Razeghi O, Gould J, Sidhu BS, Sieniewicz B, *et al.* A rule-based method for predicting the electrical activation of the heart with cardiac resynchronization therapy from non-invasive clinical data. *Med Image Anal* Elsevier B.V.; 2019;**57**:197–213.

14. Karoui A, Bear L, Migerditichan P, Zemzemi N. Evaluation of Fifteen Algorithms for the Resolution of the Electrocardiography Imaging Inverse Problem Using ex-vivo and in-silico Data. *Front Physiol* 2018;**9**.

15. Duchateau J, Sacher F, Pambrun T, Derval N, Chamorro-Servent J, Denis A, *et al.* Performance and limitations of noninvasive cardiac activation mapping. *Heart Rhythm* 2019;**16**:435–42.

16. Bear LR, Huntjens PR, Walton RD, Bernus O, Coronel R, Dubois R. Cardiac electrical dyssynchrony is accurately detected by noninvasive electrocardiographic imaging. *Heart Rhythm* Elsevier Inc.; 2018;**15**:1058–69.

17. Niederer SA, Lumens J, Trayanova NA. Computational models in cardiology. *Nat Rev Cardiol* Springer US; 2018;**16**:100–11.

18. Duchateau J, Potse M, Dubois R. Spatially Coherent Activation Maps for Electrocardiographic Imaging. *IEEE Trans Biomed Eng* 2017;**64**:1149–56.

19. Gold MR, Singh JP, Ellenbogen KA, Yu Y, Wold N, Meyer TE, *et al.* Interventricular Electrical Delay Is Predictive of Response to Cardiac Resynchronization Therapy. *JACC Clin Electrophysiol* 2016;**2**:438–47.

Tables

Table 1: Characteristics of the patients.

Patient ID	Sex	Age [y]	Scar	ECG	QRSd [ms]	TST [ms]	TAT [ms]
1	F	72	No	LBBB, SR	139	39	30
2	M	69	No	LBBB, AF	179	59	59
3	M	79	Yes (8)	IVCD, SR	138	3	3
4	M	57	Yes (6)	IVCD, SR	126	14	14
5	F	68	No	LBBB, SR	185	69	69
6	M	53	No	LBBB, SR	165	50	50
7	F	67	No	LBBB, SR, AVB1	156	72	72
8	M	68	No	LBBB, SR	154	54	54
9	M	73	Yes (1)	LBBB, SR, AVB1	176	77	77
10	M	84	No	LBBB, SR, AVB1	180	50	50
11	M	69	No	LBBB, SR, AVB1	170	68	68
	73% M	69±8.7	27% Yes	82% LBBB	160.7±18.81	50.45±22.6	49.6±24.3

Statistics are reported in the last row as average ± standard deviation for numerical data and as percentage for categorical data. Abbreviations: QRSd, QRS complex duration; TST, trans-septal time; TAT, total activation time; LBBB, left bundle branch block; SR, sinus rhythm; AVB1; atrioventricular block first degree; IVCD, intraventricular conduction delay.

Table 2: Correlation between electroanatomic maps (EAMs) and reconstructed activation times for all points in the LV and RV endocardium and LV epicardium in all patients.

Patient ID	LV endo	LV epi	RV endo	Overall
1	0.953	—	—	0.953
2	0.903	—	—	0.903
3	0.327	—	—	0.327
4	0.777	—	—	0.777
5	0.885	0.966	0.735	0.805
6	0.765	0.863	0.188	0.797
7	0.751	0.863	0.496	0.788
8	0.893	0.952	0.509	0.878
9	0.942	0.932	0.323	0.817
10	0.914	0.949	0.759	0.840
11	0.720	0.782	—	0.831
Overall	0.833	0.677	0.576	0.816

ID	I	II	III	V1	V2	V3	V4	V5	V6	aVF	aVL	aVR	all
1	0.941	0.886	0.918	0.979	0.947	0.972	0.863	0.375	0.889	0.852	0.935	0.939	0.934
2	0.191	0.920	0.928	0.849	0.885	0.991	0.949	0.754	-0.364	0.934	0.905	0.572	0.881
3	0.966	0.861	0.979	0.951	0.934	0.983	0.986	0.978	-0.301	0.958	0.984	0.432	0.944
4	0.707	0.969	0.961	0.975	0.995	0.993	0.989	0.882	0.973	0.971	0.916	0.940	0.978
5	0.899	0.623	0.879	0.968	0.996	0.986	0.981	0.469	0.646	0.799	0.919	0.630	0.963
6	0.979	0.959	0.938	0.978	0.990	0.984	0.914	0.853	0.907	0.847	0.971	0.978	0.981
7	0.800	0.591	0.935	0.964	0.991	0.940	0.930	0.759	0.246	0.852	0.942	0.341	0.843
8	0.908	0.732	0.914	0.979	0.961	0.988	0.985	0.981	0.941	0.869	0.937	-0.002	0.935
9	0.872	0.819	-0.687	0.967	0.937	0.982	0.975	0.817	0.306	0.518	0.081	0.864	0.917
10	0.870	0.858	0.418	0.941	0.953	0.946	0.622	0.767	0.905	0.622	0.819	0.878	0.932
11	0.918	0.930	0.666	0.981	0.978	0.956	0.877	-0.198	0.840	0.892	0.846	0.931	0.940
all	0.855	0.845	0.833	0.923	0.956	0.940	0.936	0.687	0.555	0.830	0.852	0.842	0.923

Table 3: Correlation between recorded and fitted ECG, grouped by patient and lead.

Figure captions

Figure 1 (Summary of the method). The workflow starts with the CMR acquisition of the anatomy of the heart and the torso (with electrode positions) and the standard 12-lead ECG (blue box). In the pre-processing phase (yellow box), a 3D anatomy of the patient is reconstructed from CMR/CT sequences. The parameter identification phase (light green box) aims at fitting the parameters of the model (CVs and EASs), to minimize the difference between recorded and simulated ECG. The reconstructed activation map was eventually validated against invasive EAM (dashed light blue box).

Figure 2 (Illustrative reconstruction). Example of the activation reconstruction for patient #4. A: recorded (blue) and fitted (orange) ECG. B: 3D view of the activation map with collected EAM points. C: LV bull's-eye plot (scar in purple.)

Figure 3 (Validation against invasive mapping). Bull's-eye plots for each patient showing the EAR (blue) and LAR (red) in the LV. The solid-colored regions refer to the recorded maps, while the hatched-colored regions are the reconstructed ones. Scar is in purple. BPs are marked by stars.
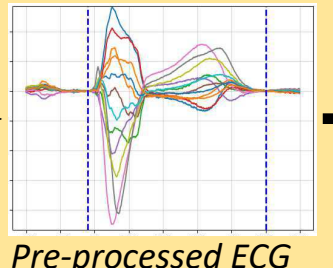
CT/CMR

Heart
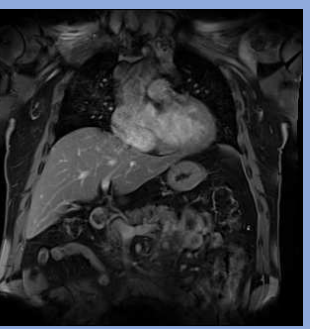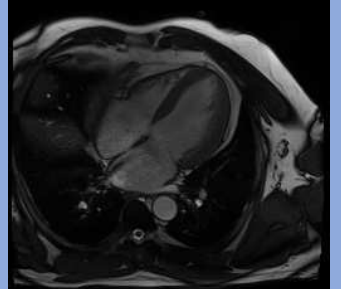
12-lead ECG
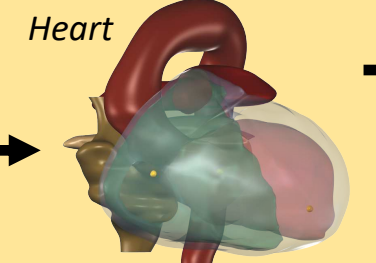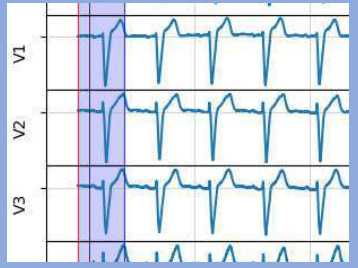
Segmentation

Torso, electrodes

Pre-processed ECG

Eikonal model

Simulate Activation

Lead-field

Simulate ECG

Compare

I   aVR   V1

Optimize EASs

Optimize CVs

Final activation map

CS

LV

RV

3D EAM

Anterior

Septum   Lateral

Inferior
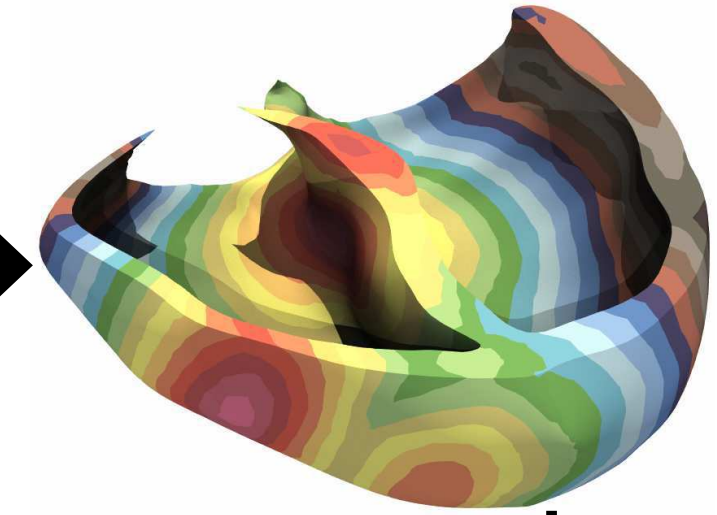
Acquisition   **Pre-processing**   **Parameter identification**   **Validation**

A — 12-lead ECG panels: I, aVR, V1, V4, II, aVL, V2, V5, III, aVF, V3, V6

B — Posterior epicardial view; Anterior epicardial view

C — Anterior / Septum / Lateral / Inferior polar map

Latest recorded and reconstructed activation

Earliest Reconstructed BT

Distance is 16 mm

Earliest Recorded BT

Scar